ADVANCED MATERIALS
www.advmat.de

Chiral Transition Metal Oxides: Synthesis, Chiral Origins, and Perspectives

Yiwen Li, Xiongbin Wang, Jun Miao, Jiagen Li, Xi Zhu, Rui Chen, Zikang Tang, Ruikun Pan, Tingchao He,* and Jiaji Cheng**

Transition metal oxides (TMOs) consist of a series of solid materials, exhibiting a wide variety of structures with tunability and versatile physicochemical properties. Such a statement is undeniably true for chiral TMOs since the introduction of chirality brings in not only active optical activities but also geometrical anisotropy due to the symmetry-breaking effect. Although progressive investigations have been made for accurately controlled synthesis and relevant explanations on the chirality origin of such materials, the overall field of chiral TMOs is still in its infancy with adequate space for interdisciplinary communications and development. Herein, therefore, recent advances in both experimental phenomena and theoretical calculations in this area are reviewed, to elucidate the underlying chiral origin with respect to their fabrications process, triggering new insights for further evolution of this field.

1. Introduction

Chirality refers to a structure lack of symmetry elements (S_n), such as mirror plane (σ) and inversion (i) symmetry, like most of chiral organic molecules in which chiral centers are surrounded by four different bonding groups.[1] Recently, the concept of chirality has extended from organic molecules to inorganic nanocrystals (NCs) whose unique physicochemical properties could be easily tuned by altering their size, shape, or ingredient, providing a powerful platform for exploring enhanced chiroptical effects, chirogenesis, and potentials in which chiral inorganic NCs could provide to interdisciplinary fields such as optical and biosensing,[2,3] chiral bioimaging,[4] and polarization-based display devices.[5] In general, chirality in inorganic NCs can be obtained from:[6,7] 1) intrinsic chirality formed by chiral crystals, lattice distortions, and defects,[8–10] 2) chiral shape with subwavelength dimensions,[11] 3) chirality transfer via chiral assembled nanostructures of achiral NCs,[5,12] and 4) chiral interactions of achiral NCs with chiral molecules[13] as depicted in **Figure 1**. The most famous property of chiral nanostructure is the optical activity which refers to the ability of a chiral unit to rotate the plane of plane polarized light.[14] In modern optics, this property is associated to the circular dichroism (CD) phenomenon, which concerns the absorption difference between left and right circularly polarized (LCP and RCP) light, therefore CD-based spectroscopies are generally regarded as powerful tools to detect chirality of a measured sample.

With rapid development, a number of cutting-edge work concerning on chiral metal nanoparticles (NPs), chiral semiconductor NCs, chiral ceramics, and metal coordinate systems has been investigated recently.[6] Among them, chiral transition metal oxides (TMOs) are a newly discovered area attracting tremendous attentions because of their striking feature for non-stoichiometry even though great challenges on establishing systematic control over the synthesis and theoretical supports for chirality induction mechanisms still remain. Since the nature of metal–oxygen bonding in TMOs can vary from nearly ionic to covalent or metallic, the physicochemical properties of TMOs are strongly related to their outer d electrons.[15] When combined with chiral molecules, the overlap of the orbital of chiral molecules with the density of states of TMOs or formation of chiral surfaces can bring in tunable chirality for TMOs from UV–visible to near infrared region, endowing fascinating chiroptical properties. Therefore, herein, we emphasize recent progress on chiral TMOs in terms of their synthesis, CD effects, and possible mechanisms of induced optical chirality. In Section 2, theoretical background on the origin of induced chirality in TMOs nanostructures is briefly introduced. Section 3 will show recent progress of chiral TMOs with their synthetic

Dr. Y. Li, Prof. R. Pan, Prof. J. Cheng
School of Materials Science and Engineering
Hubei University
Wuhan 430062, China
E-mail: rkpan@hubu.edu.cn; jiajicheng@hubu.edu.cn
X. Wang, Prof. R. Chen
Department of Electrical and Electronic Engineering
Southern University of Science and Technology
Shenzhen 518055, China
X. Wang, J. Miao, Prof. Z. Tang
Institute of Applied Physics and Materials Engineering
University of Macau
Taipa, Macau 999078, China
J. Li, Prof. X. Zhu
Shenzhen Institute of Artificial Intelligence and Robotics for Society (AIRS)
Shenzhen, Guangdong 518172, China
Prof. T. He, Prof. J. Cheng
College of Physics and Optoelectronic Engineering
Shenzhen University
Shenzhen 518060, China
E-mail: tche@szu.edu.cn
The ORCID identification number(s) for the author(s) of this article can be found under https://doi.org/10.1002/adma.201905585.

DOI: 10.1002/adma.201905585

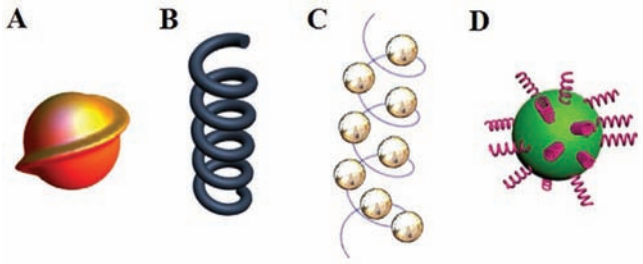

Figure 1. Inorganic nanostructures with chirality: A) intrinsically chiral NCs or lattice, B) nanostructures with chiral shape, C) chiral arrangement of achiral nanoparticles, and D) achiral nanoparticle capped with chiral molecules on the surface. A) Reproduced with permission.[8] Copyright 2012, American Chemical Society.

methods and chiral origin. Finally, Section 4 will briefly summarize the applications and potential perspectives of this research area with challenges that remain unsolved to date.

2. Chirality Theory in TMO Nanostructures

Admittedly, with more than two decades for the development of chiral TMOs, a body of extensive work focusing on TMOs with chiral shapes or chiral ligands has been reported in both micro- and nanoscale, as sketched in Figure 1. Principally, these two levels of induced chirality both express CD activities and play critical roles for understanding of the chirality induction mechanisms. Generally, the CD signal could be[16]

$$\mathrm{CD}_q = \sigma_q^{\mathrm{L}} - \sigma_q^{\mathrm{R}} \tag{1}$$

where q is the light propagation direction, and σ_q^{ε} is the absorption of (left/right) polarized light

$$\sigma_q^{\varepsilon}(\omega) = -\frac{4\pi}{c}\omega \mathrm{Im}\sum_{nm}(\varepsilon^{*}\cdot\mu_n)\mathrm{e}^{-i(q\cdot X_n)} \times \langle G_{nm}(\omega)\rangle \mathrm{e}^{i(q\cdot X_n)}(\mu_m\cdot\varepsilon) \tag{2}$$

where c is the light velocity, X_n is the position of nth monomer, $_n$ is the dipole moment, is the light frequency, and $G_{nm}(\ )$, representing the matrix element for the transition between ground state n and excited state m, can be determined by $G_{nm}(\ ) = \langle n|G(E_0 + \ )|n\rangle$, in which the green operator G can be expressed in the form of $G(E) = (E - (H_0 + V) + i\ )^{-1}$. H_0 is the hamiltonian without any interaction, and V is the interaction potential.

For most of the quantum CD theory in nanomaterials, the key idea is the treatment of interaction or scattering between light and matter in the given chiral geometry. The geometry determines the framework for the wavefunction,[17] and the scattering determines the rest. For example, $V \propto 1/r$ for the single edge dislocation,[18] while $V \propto 1/r^2$ for the screw dislocation,[18,19] and other $V \sim r$ scaling for the other interactions between plasmons and dipoles.[20,21]

For semiconductors with intrinsic chirality (Figure 1A), Fedorov and co-workers[17,22] pointed out the dislocation-induced chirality theory for understanding the chiral origins, demonstrating that optical activity can be inherent to many semiconductor nanowires as it is induced by chiral dislocations during their growth as

$$\Delta W = \frac{\pi}{\hbar^2}\sum_{n'l'p'}\Big(\big|\langle\psi_{n'l'p'}\big|\hat{H}_{\mathrm{L}}\big|\psi_{nlp}\rangle\big|^2 - \big|\langle\psi_{n'l'p'}\big|\hat{H}_{\mathrm{R}}\big|\psi_{nlp}\rangle\big|^2 + \big|\langle\psi_{n'l'p'}\big|\hat{H}_{\mathrm{L}}\big|\psi_{n,-l,p}\rangle\big|^2 - \big|\langle\psi_{n'l'p'}\big|\hat{H}_{\mathrm{R}}\big|\psi_{n,-l,p}\rangle\big|^2\Big)\delta(\omega - \omega_{nlp;n'l'p'}) \tag{3}$$

where $\hat{H}_{\mathrm{L}}$ and $\hat{H}_{\mathrm{R}}$ are the Hamiltonians describing the interaction of electrons with LCP and RCP light, $_{nlp;\ n'l'p'} = (\ _{n'l'p'} - \ _{nlp})\ /2m$ is the transition frequency. In this manner, quantum nanostructures such as dots, rods, and disks with screw dislocations could be all defined. And, the absolute values of the coef cients preceding the $(\ -\ _{nlp;\ n'l'p'})$ function is referred to as the CD strengths of intraband transitions.[17] Other than dislocation induced chirality, some chiral crystal structures prepared with chiral thiolated molecules showed as well intrinsic chirality, for which numerical solution of Maxwell's equations such as discrete dipole approximation (DDA) could be used to calculate their CD performance based on the orientation of asymmetric nanostructures.[10] However, it is worth to note that experimental evidence on such type of intrinsic chirality is still inadequate probably due to the dif culties in separation of chiral NCs based on current synthetic methods and high-resolution imaging for confirming the distortions at atomic level. To overcome this, a possible synthetic approach based on artificial intelligence (AI) robotics[23] is suggested in Section 4.

In fact, dislocation-induced chirality theory is also applicable in microscopic helical shapes (Figure 1B), in which Eshelby theory of dislocations[24] and lattice growth mechanisms[25] are responsible for the helical structure formation. While for the microscale up to the protein size, the quantum-mechanics method is inappropriate due to the huge size. The classic theory domains the CD calculation. The polarized light can be described by:[26] $E_{\pm} = E_0\ (\mathbf{i} \pm \mathbf{j})\exp[i(\ t - kz)]$, where +/− represents the left/right polarization. CD is defined as

$$\mathrm{CD} = \Delta A^{\varepsilon} = A^{\mathrm{L}} - A^{\mathrm{R}} \tag{4}$$

where ΔA is the absorbance difference of the light field for L/R polarization. $A^{\varepsilon} = \log(I_{\varepsilon}^0/I_{\varepsilon}) = \varepsilon_{\varepsilon}Cl$; I_{ε}^0 and I are the intensity of the incident polarization light both on the sample and after penetrating a length l through the solution with chiral materials concentration C. is the molar extinction coef cient for the solute.CD = ΔA = Δ Cl. Modern equipment usually uses Δ to report the CD value.

On the other hand, when semiconductor NCs are capped by chiral ligands (Figure 1D), the induced chirality could be a result of electronic interactions including orbital coupling between the NCs and orbital wave functions of chiral molecules, or the Coulomb interactions although it is not a dominant effect (inset of Figure 3 later). For the first mechanism, due to the microscopic feature, the most common way to treat it is to use atomistic calculations, for example, density function theory (DFT) in which the molecular chirality is transferred to the excitons in NCs through the orbital hybridization effect between the electronic states of the NCs and orbital wavefunctions of the chiral molecule.[12,27,28] While for the Coulomb interactions, as

summarized by Govorov et al., the CD activity of the NCs can be expressed as[20,29]

$$\mathrm{CD}_{\mathrm{NC}}(\omega)=\frac{\mathrm{Im}\left[\left(\hat{F}\vec{\mu}_{12}\right)\vec{m}_{21}\right]}{R^{3}}\frac{\omega-\omega_{0}}{(\omega-\omega_{0})^{2}+\Gamma^{2}}\mathrm{Im}\left[\alpha_{\mathrm{NC}}(\omega)\right] \quad (5)$$

where Im denotes imaginary part, $\vec{\mu}_{12}$ and $\vec{m}_{21}$ are quantum matrix elements of the electric and magnetic dipole operators, and and $_{0}$ are frequencies of incident photon and molecular transition. $\hat{F}$ is a dipole orientation matrix. $_{\mathrm{NC}}(\ )$ is the polarizability of NCs. While for the chiral molecule, its CD can be given as

$$\mathrm{CD}_{\mathrm{mol}}(\omega)=\mathrm{Im}\left[\left(\hat{P}\vec{\mu}_{12}\right)\vec{m}_{21}\right] \quad (6)$$

where $\hat{P}$ is the field enhancement factor, which means the chiral response of the molecule is affected, in return, by the semiconductor core through the refractive index.

In addition, like chiral assembly of achiral metal NPs (Figure 1C) whose overall collective chirality can be attributed to the plasmon–plasmon couplings, similar explanation on achiral semiconductor NPs assembled in a chiral manner should be acceptable as well. However, since such type of chirality is rarely reported in TMOs for the moment, we prefer to rule out this theoretical part to avoid redundancy, but some related literature is suggested for interested readers.[29,30]

3. Synthesis Methods and Chiral Origins of TMOs

In this section, we focus on different types of chiral TMOs in terms of their synthetic methods and how chirality is originated. With great efforts on the systematic control over the bench-top chemical synthesis, it is now possible to manipulate the configuration of chiral inorganic nanostructures from simple dots to rods, flowers, and more complicated helical shapes. Although the synthesis of TMOs with chiral shapes can go back a long way with various types of methods such as soft templating, 2D or 3D lithography and chemical/physical depositions, as a milestone, the ligand-induced chirality is firstly reported in the gold–glutathione nanoclusters by Schaaff and Whetten[31] until 2000, which opens a floodgate for discovering the origin of electromagnetic response between light and optically active matter with a purpose for materials' design with unique properties, especially for nanostructures based on TMOs on account of their universal feature.

3.1. TMOs with Chiral Shapes

As mentioned in the introduction, chiral TMOs exist widely in the realm of materials chemistry with various shapes and morphologies. To obtain a chiral configuration, advanced nanotechnology with top-down and bottom-up strategies are frequently employed and sometimes mutually applied. Che and co-workers,[32] for instance, reported that chiral ZnO films with a hierarchical nanostructure can be achieved via using both chemical deposition and seed growth methods, and the synthesized chiral ZnO film exhibited three levels of hierarchical chirality, including intrinsic helical ZnO crystalline chirality, helical stacking of ZnO crystalline nanoplates, and circinate aggregates formed by stacked ZnO nanoplates (**Figure** 2A, top). Further, Yeom et al.[33] demonstrated that 3D chiral plasmonic nanostructures with chiroptical activity can be achieved via using achiral ZnO nanopillars as substrate cooperated with deposition of asymmetric gold nanoshells as illustrated in the bottom panel of Figure 2A. Interestingly, they found that the asymmetric electrostatic field generated by the chiral Au nanoshells could affect the motion of carriers in ZnO nanopillars and hence transfer the geometrical chirality of the Au nanoshells to the achiral ZnO nanopillars. Meanwhile, in the work by Park and co-workers,[34] it was claimed that single-crystalline cubic helical $ZnGa_2O_4$ nanostructures can be obtained by thermal evaporation and the growth direction of $ZnGa_2O_4$ nanostructures is strongly related to the lattice matching with the ZnSe nanowires (Figure 2B), which provides an alternative angle for study on the blue-light-emitting $ZnGa_2O_4$ nanowires.[35]

Unlike zinc-based nanomaterials, molybdenum-based TMOs are widely applied in spectrum analysis, catalysis, and photothermal therapies, and in fact, MoO_3 nanostructures with chiral configurations are achieved as well. Li et al.[36] showed that helical MoO_3 nanosheets can be observed during the time-dependent oxidation reaction of MoO_3 and hydrogen peroxide. The evolution of MoO_3 morphologies is affected by the molar ratio of molybdenum and H_2O_2, and more importantly the reaction time. As illustrated by the scanning electron microscopy (SEM) images in Figure 2C, left-handed and right-handed single helical MoO_3 nanosheets can be observed at 180 °C for 6 h reaction, and afterward, such chiral shape will merge into nanoflowers to nanobelts on increasing the reaction time. Very recently, a detailed study reported by Tang and co-workers[37] described the synthesis of biomimetic chiral photonic crystals via Langmuir–Schaefer assembly of $NiMoO_4 \cdot xH_2O$ nanowires with slow alignment as shown in Figure 2D. The fabricated nanostructures showed an intricate helical structure and biomimetic circularly polarized color reflection like beetles. Additionally, since the chiral film is made by layer-by-layer technique, the chiroptical response is highly programmable (Figure 2D, bottom panel), which may give rise to chirality-based nanoscale coding and decoding for information technology in future.

Compared to macroscopic fabrication techniques, the organic templating method is considered as an economic bottom-up approach for inorganic nanomaterials synthesis with precise control over the morphology. Recently, Yang's group[38] synthesized chiral zirconia nanotubes through a sol–gel transcription approach. Thanks to the chiral low-molecular-weight gelators (LL- or DD-12Val5PyClO$_4$), the organic chirality can be transcripted to the zirconia nanotubes and the chiral morphology of the helical nanotubes is found to be sensitive to the gelation time (Figure 2E). Similarly, helical tantalum oxide nanostructures are obtained as well. Hanabusa and co-workers[39] exhibited tantalum oxide helices can be created by a sol–gel polymerization of metal alkoxides using the chiral aggregates of supramolecular organogelators (Figure 2F). Later, Yang

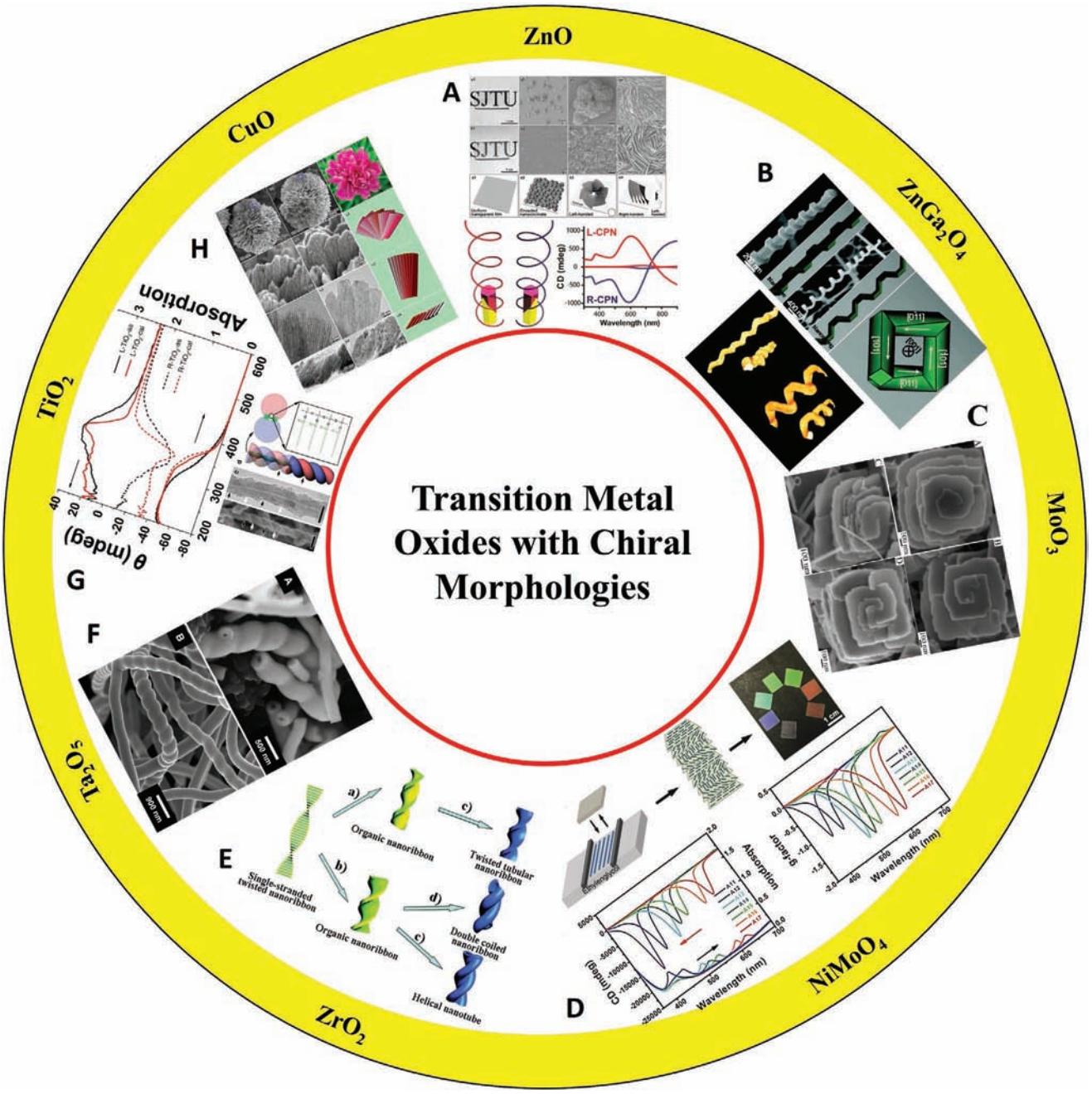

Figure 2. TMOs with chiral shapes. A) Top: SEM images and sketches of chiral ZnO films with a hierarchical nanostructure. Reproduced with permission.[32] Copyright 2015, Wiley-VCH. Bottom: Chiral ZnO nanopillars with chiral gold nanoshells and their CD spectrum. Reproduced with permission.[33] Copyright 2013, American Chemical Society. B) TEM images of helical $ZnGa_2O_4$ nanowires and top-view diagram showing the four growth directions of the helical nanowires. Reproduced with permission.[34] Copyright 2005, American Chemical Society. C) SEM images of helical MoO_3 nanostructures synthesized at 180 °C for 6 h (the molar ratio of molybdenum and H_2O_2 is 0.17). Reproduced with permission.[36] Copyright 2006, American Chemical Society. D) Top: Sketches of Langmuir–Schaefer assembly of $NiMoO_4{\cdot}xH_2O$ nanowires for chiral photonic crystals and their optical images under a right circular polarizer. Bottom: CD and *g*-factor of seven samples with a full pitch containing anticlockwise rotated 11–17 nanowire film layers, respectively. Reproduced with permission.[37] Copyright 2019, Wiley-VCH. E) Schematic presentation of the formation of the right-handed helical ZrO_2 nanostructures. Reproduced with permission.[38] Copyright 2014, Royal Society of Chemistry. F) SEM images of tantalum oxide fibers obtained from chiral aggregates of supramolecular organogelators (top) and its enantiomer (bottom). Reproduced with permission.[39] Copyright 2002, American Chemical Society. G) SEM images, TEM images, and schematic drawings of the as-prepared organic-lipid–TiO_2 hybrid fibers synthesized with R-TiO_2-as and DRCD spectra of antipodal as-prepared and calcined samples. Reproduced with permission.[41] Copyright 2012, Springer Nature. H) SEM and HRTEM images and schematic drawings of sinistrorse CuO nanof owers with dif erent morphologies. Reproduced with permission.[42] Copyright 2014, American Chemical Society.

demonstrated that the recorded optical activity in CD measurement is irrelevant to the handedness of the Ta_2O_5 nanotubes. Further simulations based on time-dependent density functional theory (TD-DFT) indicated that chiral point defects were responsible for the optical activity.

Intuitively, since the development of sol–gel chemistry,[40] soft templating synthesis of metal oxides such as Azo, titania, and TMOs are widely performed. Liu et al.[41] for example, reported the synthesis of chiral TiO_2 fibers via fine-controlled transcription of amino acid-derived amphiphile fibers through coordination bonding interactions between the organics and the TiO_2 source. In addition, since the observed optical activities are located in the band edge region, the chiral origin is considered as the result of asymmetric electronic transitions of semiconducting TiO_2 with CD activities (Figure 2G).

By learning from the flower-like structures in nature, which express helical symmetry with a rotation of contort petal aestivation, the conceptual chirality of nanoflowers was achieved in recent year by the Che's group.[42] Through surfactant-mediated hydrothermal reaction, chiral CuO nanoflowers can be obtained by applying cupric salt as CuO source and sodium dodecyl sulfate as the structure-directing agent. The hierarchical chirality exhibited by the nanoflakes and the nanopetals with helically arranged sub-nanopetals in Figure 2H are regarded as the two major chiral origin. Thereafter, their follow-up work[43] utilized these chiral flowers to form chiral CuO films by chemical deposition. The synthesized CuO chiral film exhibited both optical activities at band-edge achieved by the electron transition, and reflection chirality at circular Bragg resonance induced by long range periodic structure, providing new understanding of the links between the chiral configurations and the optical properties.

3.2. TMOs with Ligand-Induced Chirality

Theoretically, when TMOs are capped with chiral ligands, chiroptical responses in CD spectra can be originated from two possible types of symmetry breaking effects: i) intrinsically chiral core with dislocations and defects; ii) ligand-induced chiral surfaces, defects, or chiral interactions between chiral ligands and achiral core. For the chiral interactions, orbital coupling and Coulombic interaction are basically accepted as the very possible mechanisms for chirality-transfer as depicted in **Figure 3**.[29] Yeom et al.[44] reported when Co_3O_4 NCs are capped by chiral ligands such as l- and d-cysteine or penicillamine, strong chiroptical response with anisotropy *g*-factors as high as 0.02 can be obtained (Figure 3A, middle panel). With the help of advanced simulation techniques such as TD-DFT and ab initio molecular dynamics (AIMD) (Figure 3A, top panel), chiral distortion of the original cubic spinel lattice induced by the overlap between atomic orbitals of Co^{3+} and O^{2-} is revealed eventually as the chirogenesis. In light of the strong CD activities of chiral Co_3O_4 nanoparticles, chiral WO_{3-x} nanoparticles was synthesized by Kotov and co-workers[45] with the same chirality transfer approach. Different from metal–S bond linkage, amino acids, typically aspartic acid (Asp) and proline (Pro) molecules, are selected as chirality inducing ligand to WO_{3-x} nanoparticles surface through C–O–W linkages with slight coordination as shown in Figure 3B. Two types of chirality are observed in the chiral WO_{3-x} nanoparticles, i.e., the metal-to-ligand charge transfer (MLCT) chirality at visible region, and the plasmonic chirality at near infrared band. As illustrated by MD simulations in Figure 3B, the dihedral angles show that lattice distortion is introduced when chiral ligands such as Asp is linked to the semiconductor core, and further CD observations indicate that such optical activity is greatly related to the binding mode of the amino acids where Asp has one additional C–O–W linkage compared to Pro resulting in stronger distortion of the inorganic crystal lattice and greater intensity of CD bands.[45]

Inspired by the MLCT chirality, our recent work presents that chiral MoO_{3-x} nanoparticles can be achieved via using cysteine molecules as reducing and capping agent.[27] As shown in Figure 3C, through the oxidation reaction, MoS_2, as the Mo source, can be oxidized into Mo^{VI} and then chiral cysteine molecules are applied as the reducing agent to obtain chiral MoO_{3-x} nanoparticles with different valence states. As the reduction continues, the chiral MoO_{3-x} nanoparticles express blue color with plasmonic chirality at near infrared region, and then green and brown colors with strong MLCT chirality at visible band (≈580 nm) as indicated by the UV and CD spectra in Figure 3C. However, our TD-DFT simulations show that the MLCT band transition is contributed by the transition from the metal complexing ligand-based orbitals and ligand-based * orbitals. Such MLCT chirality gives a new scope for the chiral interactions between the metal core and chiral ligands and also provides a versatile toolbox for chiral semiconductor nanosensors, optoelectronics, and photocatalysis.

With the know-how that chiral molecules are favored for surface functionalization of TMOs, many biological issues such as cytotoxicity and biocompatibility can be sometimes improved. Recent work by Kuang and Xu[2] proves that Cu_xO nanoparticles surface modified with chiral molecules can serve as an antioxidant for ameliorating Parkinson's disease. As shown in Figure 3D, after achiral Cu^{II} is coordinated with phenylalanine and treated with d-glucose, Cu_xO nanoparticles can be formed via slight reduction. With this surface modification, the chiral phenylalanine-capped Cu_xO nanoparticles shows small size (≈65 nm, Figure 3D bottom panel) with no observable cytotoxicity and strong reactive oxygen species (ROS) elimination performance which is a critical signal for relieving Parkinson's disease. Nevertheless, it is worth to mention that no clear CD signals were shown in this nanostructure, which is probably due to the detection limit of CD spectrometer in near infrared region for doped semiconductor NCs with surface plasmon resonance (SPR) effects.

In order to observe electronic transitions in the UV–visible range, Gun'ko and co-workers[46] reported that (1R,2R)-(+)-1,2-diphenylethylenediamine or (1S,2S)-(−)-1,2-diphenylethylenediamine-capped TiO_2 nanoparticles with dendritic morphology shows CD activity at the TiO_2 bandgap and a photoluminescence quantum yield of 3.5% (Figure 3E), in which, as expected, the origin of the chirality is related to the ligand-induced effect caused by the overlap of the chiral ligand highest occupied molecular orbitals (HOMOs) with the nanoparticles valence band states but not caused by a chiral surface or defects. Although no study on the circularly polarized luminescence (CPL) of such materials is mentioned in this work probably due

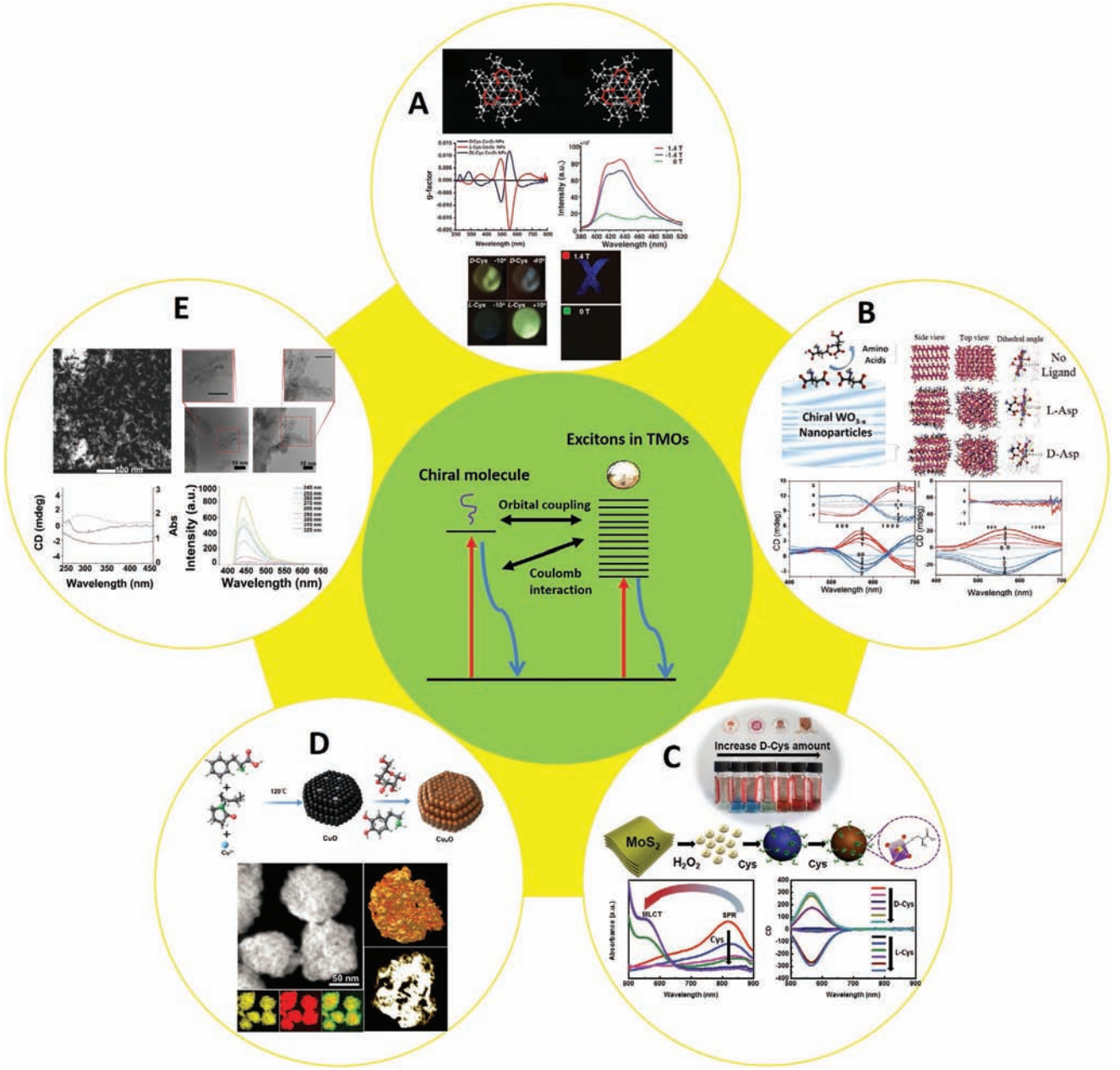

Figure 3. A) Top: Rotations of crystalline structures of d- and l -cysteine-capped Co_3O_4 NCs. Middle: *g*-Factor curves of d-, l -, and dl -cysteine-capped Co_3O_4 NCs (left) and emission intensities of f uorescent paper plus the NCs gel in front with a magnetic field (red and blue) and without a magnetic field (green) (excitation, 280 nm). Bottom: Photographs of light transmission through the NCs, with the rotation of the linear analyzer counterclockwise (–10°), and clockwise (+10°) (left), and photographs of blue-emitting light from the f uorescent paper. Adapted with permission.[44] Copyright 2018, American Association for the Advancement of Science. B) Top panel: Sketches of chiral amino acids interact with WO_{3-x} NCs for induced chirality (left) and MD simulations of the atomic structure in the minimum energy state for ligand-free, l -Asp, and d-Asp NCs. Bottom: CD spectra of l - and d-Asp-NCs (red and blue) (inset: NIR range of corresponding CD spectra) and l - and d-Pro-NCs (red and blue) (inset: NIR range of corresponding CD spectra) containing dif erent concentrations of water. Reproduced with permission.[45] Copyright 2017, American Chemical Society. C) Top: Illustration of the synthesis of chiral MoO_{3-x} NCs and their real images. The dif erent amounts of cysteine could reduce the MoO_3 to obtain various cationic valence. Reproduced with permission.[27] Copyright 2018, Wiley-VCH. D) Top: Schematic illustration of the preparation of Cu_xO NCs via chiral molecules. Bottom: HRTEM images with STEM and energy-dispersive X-ray spectroscopy (EDS) mapping, and 3D electron tomography reconstruction images of Cu_xO NCs prepared using l -phenylalanine. Reproduced with permission.[2] Copyright 2019, American Chemical Society. E) Top: STEM (left) and TEM (right) images of (+)-diphenylethylenediamine-capped TiO_2 nanoparticles. Black scale bars represent 10 nm. Bottom: (Left) CD spectra (blue) and absorption spectra (black) of (+)-diphenylethylenediamine- (solid) and (–)-diphenylethlenediamine- (dotted) capped TiO_2 nanoparticles. (Right) Excitation spectra of (+)-diphenylethylenediamine-capped TiO_2 nanoparticles. Reproduced with permission.[46] Copyright 2017, Wiley-VCH.

to the low accessibility for experimental equipment, the broad emission properties induced by the chiral surface modification unveiled its promising potential for chiral optoelectronic devices.

4. Applications and Perspectives

Chiral TMOs, as a newly flourishing field, have been greatly developed over the past two decades. The introduction of chirality to TMOs has revolutionized the motif of TMOs with respect to their applications in area of chiroptical sensing and detection, enantioselective catalysis, biological-tissue-based therapy, and chirality-based devices. Since a body of related reviews has well summarized the details about the possible applications of chiral inorganic NCs,[6,47–55] we would prefer only to highlight some representative examples of chiral TMOs here:

1) Chiroptical sensing and detection: Xu and co-workers[56] reported recently that chiral CuxOS@ZIF-8 nanostructures can be used as ultrasensitive probe for detection of H_2S in vivo with the limit of detection of 0.3×10^{-9} and 2.2×10^{-9} m for CD and fluorescence methods because H_2S can reduce the chiroptical intensity and increase the fluorescent signal of the nanostructures (**Figure** 4A). Jiang's group[57] also demonstrated that cysteine-capped Au/Fe_3O_4 NPs can enantioselectively detect the percentage of d-tyrosine in a mixture of enantiomers via cysteine as the chiral selector.
2) Enantioselective catalysis: Qu and co-workers[58] developed phenylalanine-modified cerium oxide nanoparticles (CeNPs) as chiral nanozyme for stereoselective oxidation of 3,4-dihydroxyphenylalanine (DOPA) enantiomers where l-CeNP showed higher catalytic ability for oxidation of d-DOPA while d-CeNP were more effective to l-DOPA (Figure 4B). In addition, Kotov "and co-workers[45] as mentioned in Figure 3B exhibited that nonstoichiometric WO_{3-x} NPs are capable for peptide catalysis.
3) Chiral nanophotonics: Deng and co-workers[59] have highlighted that CuO/cellulose crystal (CNC) and CuO (calcinated from CuO/CNC) nanoflowers can both serves as chiral template for generating full-color CPL when achiral fluorescent dyes are mixed with them (Figure 4C). Besides, Kotov's recent work,[44] as shown in Figure 3A, pointed out that chiral Co_3O_4 gels can realize optical modulation via a magnetic field leading to strong absorption variation.
4) Chirality-based therapy: Our work on nonstoichiometric chiral MoO_{3-x} NPs[60] showed both visible- and NIR-light selective absorption due to the chirality induction by surface chiral ligands, which enables chiral MoO_{3-x} NPs as dual-mode photothermal therapy (PTT) agents for cancer treatments (Figure 4D). Similarly, Kuang's work[2] as previously discussed, showed that phenylalanine-capped Cu_xO NPs can be

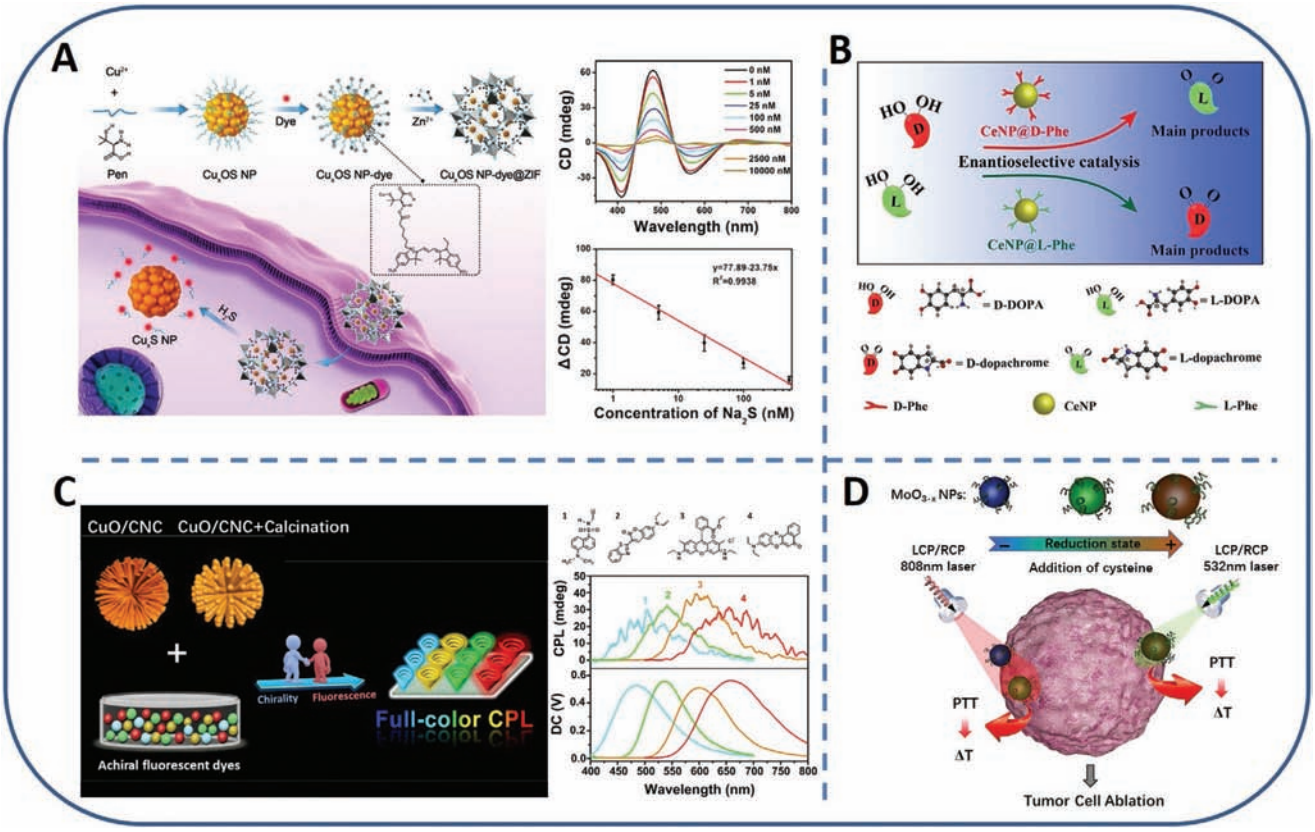

Figure 4. Typical applications of chiral TMOs. A) Chirality-based sensing of H_2S in vivo by chiral Cu_xOS@ZIF-8 nanostructures. Reproduced with permission.[56] Copyright 2020, Wiley-VCH. B) Scheme of enantioselective catalysis of DOPA and enantiomers via chiral CeNPs. Reproduced with permission.[58] Copyright 2020, Wiley-VCH. C) Full-color generation of CPL via using CuO/CNC and CuO (calcinated from CuO/CNC) nanof owers as template mixed with achiral organic dyes (1–4). Reproduced with permission.[59] Copyright 2020, American Chemical Society. D) Scheme of chirality-based PTT of HeLa cells via chiral MoO_{3-x} nanoparticles with dif erent reduction valence. Reproduced with permission.[60] Copyright 2020, Wiley-VCH.

used to scavenge ROS in vivo, therefore rescued the memory loss of mice with Parkinson's disease.

5) Chirality-based devices: As mentioned in Figure 2D, the layer-by-layer nanostructure of chiral $NiMoO_4 \cdot xH_2O$ photonic crystals reported by Tang and co-workers[37] exhibited extremely large chiroptical activity ($g_{max} \approx -1.6$) with tunable features providing possibilities for chirality-based multifunctional devices with favorable optical, electrical, and magnetic properties.

It is however worth noting that the development of chiral TMOs is still in its infancy. Interdisciplinary studies are still needed for expanding chiral synthesis, chiral light–matter interactions, and quantum-mechanics theories to trigger experiments on innovative materials design, pushing researchers to re-evaluate the origin of electromagnetic response between light and chiral matters so as to discover newly released areas with new applications and challenges. In particular, a perspective about the future development on chiral synthesis, theoretical simulations, and possible applications is outlined as below:

1) Chiral synthesis: Although many chiral TMO nanostructures are reported in previous sections, scientific demands for extending the breadth of enatiomerically controlled synthesis of chiral TMOs with tunable shapes, large-scale, and unique physicochemical properties are overwhelmingly at the top of the wishlist.[61] In fact, unlike other chiral inorganic nanostructures such as gold and silver, TMOs with intrinsic chiral lattice and collective chiral assembly of achiral TMOs nanostructures (Figure 1A,C) are rarely discovered. Therefore, more advanced and smart fabrication techniques with fine control over the synthesis of chiral TMOs are imperative. One possible approach reported recently by Zhu's group[23] is to employ AI robotic systems equipped with a pump–probe laser and CD spectrometer as an in situ deep-learning modulator for real-time management of chiral synthesis. This method has proved to be an efficient way for obtaining enantioselective chiral perovskite, in which it is usually difficult to observe distortions and screw-dislocations, let alone chiral separations from their enantiomers.
2) Theoretical simulations: Consider the complicated physics behind chirality and inorganic nanomaterials, many advanced theoretical simulation methods such as DDA, coupled dipole method (CDM),[62] DFT,[28] AIMD,[45] and nondegenerate coupled-oscillator (NDCO)[13] are applied for modeling with a purpose to unveil the chiral origins and obtaining CD lineshapes. Indeed, these simulations are a strong call for experimental verification, however, they are also imperfect with shortcomings. DFT or TDDFT, for instance, generally uses atomistic models however NPs in reality consist of thousands of atoms, which is hard to be processed by such method. It is therefore well-expected that future development on quantum-mechanic theories would provide a more detailed and reliable explanation on optical activity of chiral inorganic nanostructures.
3) Potential applications: As mentioned before, there have already been a great number of applications of chiral TMOs in the area of chiroptical sensing, enantioselective catalysis, and chirality-based therapy and devices. However, the majority of these existing applications are related to chemical and biological issues. More optical and optoelectronic features such as CPL generation, linear and nonlinear optical properties, photovoltaics, ferroelectricity, and spintronics may be the theme for next generation of chiral TMOs related nanomaterials' design.[63–65]

In summary, although lots of fascinating properties of chiral TMOs are only now being explored, modulated, and applied in multidisciplinary areas, it is very likely the development of innovative materials related to chiral TMOs will be fruitful as the synthetic approaches mature even further with more advanced theoretical support.

Acknowledgements

Y.L. and X.W. contributed equally to this work. The work was supported by the open research fund of Key Laboratory for Organic Electronics and Information Displays, the Natural Science Foundation of Guangdong Province (2019A1515012094), and Shenzhen Basic Research Project of Science and Technology (JCYJ20190808121211510).

Conflict of Interest

The authors declare no conflict of interest.

Keywords

chiral origin, induced chirality, nanocrystals, transition metal oxides

Received: August 28, 2019
Revised: April 17, 2020
Published online: August 2, 2020

[1] J. Cheng, E. H. Hill, Y. Zheng, T. He, Y. Liu, *Mater. Chem. Front.* **2018**, *2*, 662.
[2] C. Hao, A. Qu, L. Xu, M. Sun, H. Zhang, C. Xu, H. Kuang, *J. Am. Chem. Soc.* **2019**, 141, 1091.
[3] M. L. Solomon, A. A. E. Saleh, L. V. Poulikakos, J. M. Abendroth, L. F. Tadesse, J. A. Dionne, *Acc. Chem. Res.* **2020**, 53, 588.
[4] R. Gao, L. Xu, C. Hao, C. Xu, H. Kuang, *Angew. Chem., Int. Ed.* **2019**, 58, 3913.
[5] L. Xu, M. Sun, W. Ma, H. Kuang, C. Xu, *Mater. Today* **2016**, 19, 595.
[6] W. Ma, L. Xu, A. F. de Moura, X. Wu, H. Kuang, C. Xu, N. A. Kotov, *Chem. Rev.* **2017**, 117, 8041.
[7] A. Ben-Moshe, B. M. Maoz, A. O. Govorov, G. Markovich, *Chem. Soc. Rev.* **2013**, 42, 7028.
[8] Z. Fan, A. O. Govorov, *Nano Lett.* **2012**, 12, 3283.
[9] A. Ben-Moshe, A. O. Govorov, G. Markovich, *Angew. Chem., Int. Ed.* **2013**, 52, 1275.
[10] A. Ben-Moshe, S. G. Wolf, M. B. Sadan, L. Houben, Z. Fan, A. O. Govorov, G. Markovich, *Nat. Commun.* **2014**, 5, 4302.
[11] J. K. Gansel, M. Thiel, M. S. Rill, M. Decker, K. Bade, V. Saile, G. von Freymann, S. Linden, M. Wegener, *Science* **2009**, *325*, 1513.
[12] J. Cheng, J. Hao, H. Liu, J. Li, J. Li, X. Zhu, X. Lin, K. Wang, T. He, *ACS Nano* **2018**, 12, 5341.
[13] X. Gao, X. Zhang, K. Deng, B. Han, L. Zhao, M. Wu, L. Shi, J. Lv, Z. Tang, *J. Am. Chem. Soc.* **2017**, 139, 8734.

[14] L. D. Barron, *J. Mol. Struct.* **1983**, 101, 343.
[15] A. J. Moulson, in *Concise Encyclopedia of Advanced Ceramic Materials* (Ed. R. I. Brook), Pergamon Press, Elsevier **1991**, pp. 497–499.
[16] A. Eisfeld, R. Kniprath, J. S. Briggs, *J. Chem. Phys.* **2007**, 126, 104904.
[17] A. S. Baimuratov, I. D. Rukhlenko, R. E. Noskov, P. Ginzburg, Y. K. Gun'Ko, A. V. Baranov, A. V. Fedorov, *Sci. Rep.* **2015**, 5, 14712.
[18] R. Bausch, R. Schmitz, Ł. A. Turski, *Phys. Rev. Lett.* **1998**, 80, 2257.
[19] R. Bausch, R. Schmitz, Ł. A. Turski, *Phys. Rev. B* **1999**, 59, 13491.
[20] A. O. Govorov, Y. K. Gun'Ko, J. M. Slocik, V. A. Gérard, Z. Fan, R. R. Naik, *J. Mater. Chem.* **2011**, *21*, 16806.
[21] A. O. Govorov, *J. Phys. Chem. C* **2011**, 115, 7914.
[22] A. S. Baimuratov, I. D. Rukhlenko, Y. K. Gun'Ko, A. V. Baranov, A. V. Fedorov, *Nano Lett.* **2015**, 15, 1710.
[23] J. Li, J. Li, R. Liu, Y. Tu, Y. Li, J. Cheng, T. He, X. Zhu, *Nat. Commun.* **2020**, 11, 2046.
[24] M. J. Bierman, Y. K. A. Lau, A. V. Kvit, A. L. Schmitt, S. Jin, *Science* **2008**, *320*, 1060.
[25] H.-F. Zhang, C.-M. Wang, L.-S. Wang, *Nano Lett.* **2002**, *2*, 941.
[26] G. D. Fasman, *Circular Dichroism and the Conformational Analysis of Biomolecules*, Springer, Boston, MA, USA **1996**.
[27] Y. Li, J. Cheng, J. Li, X. Zhu, T. He, R. Chen, Z. Tang, *Angew. Chem., Int. Ed.* **2018**, 57, 10236.
[28] U. Tohgha, K. K. Deol, A. G. Porter, S. G. Bartko, J. K. Choi, B. M. Leonard, K. Varga, J. Kubelka, G. Muller, M. Balaz, *ACS Nano* **2013**, 7, 11094.
[29] A. O. Govorov, F. Zhiyuan, H. Pedro, J. M. Slocik, R. R. Naik, *Nano Lett.* **2010**, 10, 1374.
[30] A. Guerrero-Martínez, J. L. Alonso-Gómez, B. Auguié, M. M. Cid, L. M. Liz-Marzán, *Nano Today* **2011**, 6, 381.
[31] T. G. Schaaf , R. L. Whetten, *J. Phys. Chem. B* **2000**, 104, 2630.
[32] Y. Duan, L. Han, J. Zhang, S. Asahina, Z. Huang, L. Shi, B. Wang, Y. Cao, Y. Yao, L. Ma, C. Wang, R. K. Dukor, L. Sun, C. Jiang, Z. Tang, L. A. Nafie, S. Che, *Angew. Chem., Int. Ed.* **2015**, 54, 15170.
[33] B. Yeom, H. Zhang, H. Zhang, J. I. Park, K. Kim, A. O. Govorov, N. A. Kotov, *Nano Lett.* **2013**, *13*, 5277.
[34] S. Y. Bae, J. Lee, H. Jung, J. Park, J.-P. Ahn, *J. Am. Chem. Soc.* **2005**, 127, 10802.
[35] S. Y. Bae, H. W. Seo, C. W. Na, J. Park, *Chem. Commun.* **2004**, 1834.
[36] G. Li, L. Jiang, S. Pang, H. Peng, Z. Zhang, *J. Phys. Chem. B* **2006**, 110, 24472.
[37] J. Lv, D. Ding, X. Yang, K. Hou, X. Miao, D. Wang, B. Kou, L. Huang, Z. Tang, *Angew. Chem., Int. Ed.* **2019**, 58, 7783.
[38] H. Huo, S. Wang, S. Lin, Y. Li, B. Li, Y. Yang, *J. Mater. Chem. A* **2014**, *2*, 333.
[39] S. Kobayashi, N. Hamasaki, M. Suzuki, M. Kimura, H. Shirai, K. Hanabusa, *J. Am. Chem. Soc.* **2002**, 124, 6550.
[40] C. J. Brinker, G. W. Scherer, *Sol-Gel Science: The Physics and Chemistry of Sol-Gel Processing*, Academic Press, Boston, MA, USA **1990**.
[41] S. Liu, L. Han, Y. Duan, S. Asahina, O. Terasaki, Y. Cao, B. Liu, L. Ma, J. Zhang, S. Che, *Nat. Commun.* **2012**, *3*, 1215.
[42] Y. Duan, X. Liu, L. Han, S. Asahina, D. Xu, Y. Cao, Y. Yao, S. Che, *J. Am. Chem. Soc.* **2014**, 136, 7193.
[43] Y. Qian, Y. Duan, S. Che, *Adv. Opt. Mater.* **2017**, 5, 1601013.
[44] J. Yeom, U. S. Santos, M. Chekini, M. Cha, A. F. de Moura, N. A. Kotov, *Science* **2018**, *359*, 309.
[45] S. Jiang, M. Chekini, Z.-B. Qu, Y. Wang, A. Yeltik, Y. Liu, A. Kotlyar, T. Zhang, B. Li, H. V. Demir, N. A. Kotov, *J. Am. Chem. Soc.* **2017**, 139, 13701.
[46] O. Cleary, F. Purcell-Milton, A. Vandekerckhove, Y. K. Gun'ko, *Adv. Opt. Mater.* **2017**, 5, 1601000.
[47] W. Ma, L. Xu, L. Wang, C. Xu, H. Kuang, *Adv. Funct. Mater.* **2019**, *29*, 1805512.
[48] X. Gao, B. Han, X. Yang, Z. Tang, *J. Am. Chem. Soc.* **2019**, 141, 13700.
[49] G. Long, R. Sabatini, M. I. Saidaminov, G. Lakhwani, A. Rasmita, X. Liu, E. H. Sargent, W. Gao, *Nat. Rev. Mater.* **2020**, 5, 423.
[50] U. Hananel, A. Ben-Moshe, D. Tal, G. Markovich, *Adv. Mater.*, https://doi.org/10.1002/adma.201905594.
[51] J. M. Fernández-García, P. J. Evans, S. Filippone, M. Á. Herranz, N. Martín, *Acc. Chem. Res.* **2019**, 52, 1565.
[52] H.-Y. Ahn, S. Yoo, N. H. Cho, R. M. Kim, H. Kim, J.-H. Huh, S. Lee, K. T. Nam, *Acc. Chem. Res.* **2019**, 52, 2768.
[53] S. Mokashi-Punekar, Y. Zhou, S. C. Brooks, N. L. Rosi, *Adv. Mater.*, https://doi.org/10.1002/adma.201905975.
[54] X. Zhao, S.-Q. Zang, X. Chen, *Chem. Soc. Rev.* **2020**, 49, 2481.
[55] Y. Dong, Y. Zhang, X. Li, Y. Feng, H. Zhang, J. Xu, *Small* **2019**, 15, 1902237.
[56] A. Yuan, C. Hao, X. Wu, M. Sun, A. Qu, L. Xu, H. Kuang, C. Xu, *Adv. Mater.* **2020**, *32*, 1906580.
[57] X. Shi, Y. Wang, C. Peng, Z. Zhang, J. Chen, X. Zhou, H. Jiang, *Electrochim. Acta* **2017**, 241, 386.
[58] Y. Sun, C. Zhao, N. Gao, J. Ren, X. Qu, *Chem. - Eur. J.* **2017**, *23*, 18146.
[59] B. Zhao, H. Yu, K. Pan, Z. Tan, J. Deng, *ACS Nano* **2020**, 14, 3208.
[60] Y. Li, Z. Miao, Z. Shang, Y. Cai, J. Cheng, X. Xu, *Adv. Funct. Mater.* **2020**, *30*, 1906311.
[61] J. Nai, B. Y. Guan, L. Yu, X. W. Lou, *Sci. Adv.* **2017**, *3*, e1700732.
[62] J. Cheng, G. Le Saux, J. Gao, T. Buf eteau, Y. Battie, P. Barois, V. Ponsinet, M.-H. Delville, O. Ersen, E. Pouget, R. Oda, *ACS Nano* **2017**, 11, 3806.
[63] T.-T. Zhuang, Y. Li, X. Gao, M. Wei, F. P. García de Arquer, P. Todorović, J. Tian, G. Li, C. Zhang, X. Li, L. Dong, Y. Song, Y. Lu, X. Yang, L. Zhang, F. Fan, S. O. Kelley, S.-H. Yu, Z. Tang, E. H. Sargent, *Nat. Nanotechnol.* **2020**, 15, 192.
[64] C. C. Homes, T. Vogt, S. M. Shapiro, S. Wakimoto, A. P. Ramirez, *Science* **2001**, *293*, 673.
[65] G. Long, C. Jiang, R. Sabatini, Z. Yang, M. Wei, L. N. Quan, Q. Liang, A. Rasmita, M. Askerka, G. Walters, X. Gong, J. Xing, X. Wen, R. Quintero-Bermudez, H. Yuan, G. Xing, X. R. Wang, D. Song, O. Voznyy, M. Zhang, S. Hoogland, W. Gao, Q. Xiong, E. H. Sargent, *Nat. Photonics* **2018**, 12, 528.